Cross-section measurements for the ^{56}Fe($n, xn\gamma$) reactions

A. Negret,[1,*] C. Borcea,[1] Ph. Dessagne,[2] M. Kerveno,[2] A. Olacel,[1,3] A. J. M. Plompen,[4] and M. Stanoiu[1]
[1] *"Horia Hulubei" National Institute for Physics and Nuclear Engineering, 077125, Bucharest-Măgurele, Romania*
[2] *CNRS, Université de Strasbourg, UMR7178, IPHC, 23 rue du Loess, 67037, Strasbourg, France*
[3] *University of Bucharest, Faculty of Physics, 077125, Bucharest-Măgurele, Romania*
[4] *European Commission, Joint Research Centre, Institute for Reference Materials and Measurements, B-2440, Geel, Belgium*
(Received 23 June 2014; revised manuscript received 12 August 2014; published 5 September 2014)

A measurement was performed at the white neutron source Geel Linear Accelerator (GELINA) of the Institute for Reference Materials and Measurements to determine the cross sections for the $(n, n'\gamma)$ and $(n, 2n'\gamma)$ reactions on ^{56}Fe. The Gamma Array for Inelastic Neutron Scattering (GAINS) was used. The results are scaled to the neutron-induced fission cross section of ^{235}U. The paper emphasizes the multiple checks performed to assure the consistency of the results. γ production cross sections, total inelastic cross sections, and level production cross sections were determined. A good agreement exists with previous measurements. Theoretical calculations were performed with the TALYS 1.6 reaction code using default parameters, but also using a microscopic approach. These calculations are discussed in comparison to the experimental data.

DOI: 10.1103/PhysRevC.90.034602 PACS number(s): 25.40.Fq, 29.30.Kv, 27.40.+z

I. INTRODUCTION

The importance of nuclear data with low uncertainties was highly emphasized during the last years. As new nuclear facilities are developed with the aim to address the energy needs of society, it becomes clear that improved neutron cross-section values are required. The effort of building data bases is driven by sensitivity studies that determine the impact of nuclear data on reactor calculations [1,2]. The main interest at this moment concerns the precise cross sections of structural materials and of other elements used in the design of the Generation-IV nuclear reactors. Inelastic scattering is particularly important as it represents the main neutron energy loss mechanism and therefore a good knowledge of the cross sections is essential for the safety, the size, and consequently the cost of the newly developed facilities.

Iron has four stable isotopes (^{54}Fe − 5.85%, ^{56}Fe − 91.75%, ^{57}Fe − 2.12%, and ^{58}Fe − 0.28%) [3] and represents an essential structural material. Therefore an entry of the Nuclear Data High Priority Request List maintained by the Nuclear Energy Agency is dedicated to the neutron inelastic cross sections on ^{56}Fe demanding a significant reduction of the cross-section uncertainties [4]. The differences among the numerous available experimental results remain significant and largely unexplained. The sensitivity studies demand accuracies lower than 5%, requiring even uncertainties of the order of 2% for the development of accelerator driven systems (ADS) [4,5]. These are far beyond the accuracy of the available data. Such a precise measurement requires special experimental conditions.

The ^{56}Fe(n, n') reaction was extensively studied. Already in 1935 an experiment of Lea dealt with the neutron-induced γ rays from Fe [6]. In 1956, Day used the γ rays detected from inelastic scattering of neutrons for spectroscopic purposes [7]. Numerous other experiments were performed over the years to study inelastic scattering of neutrons from Fe, mostly using γ spectroscopy techniques. The most important issue is the precise determination of the γ production cross section for the first transition in ^{56}Fe, $E_\gamma = 846.8$ keV. Looking through the available experimental data, we chose several representative such measurements to compare to our results: A measurement performed in 1971 by Perey *et al.* at the white neutron source Oak Ridge Electron Linear Accelerator (ORELA) facility used a hydrogen-free carbon fluoride liquid scintillator to detect the γ rays in a 4π geometry [8]. Their results cover the neutron energy range from 0.8 to about 2 MeV. A few years later Smith reported on a measurement performed at the Argonne National Laboratory Fast Neutron Generator [9]. The neutrons were produced using the ^{7}Li(p, n)^{7}Be reaction at various energies ranging from 0.93 to 2.03 MeV. A Ge(Li) detector was used to determine not only the excitation function of the 846.8-keV γ ray, but also the angular distribution. The authors concluded that, considering the angular distribution of the 846.8-keV γ ray, the attempt to infer the angle-integrated cross section based on a measurement at 125° results in significant errors. We will compare our ratio of the 110° and 150° differential cross sections to the angular distribution determined by Smith. A more recent experiment performed in 1991 at ORELA by Dickens *et al.* extended the neutron energy range up to 41 MeV [10]. The γ rays were measured at 125° using a large high-purity germanium (HPGe) detector. Nelson from Los Alamos National Laboratory (LANL) reported in 2004 on a measurement performed at Weapons Neutron Research Facility (WNR) using the Germanium Array for Neutron Induced Excitations (GEANIE) detector array with the purpose of inferring improved standards for cross-section measurements [11]. Finally, we will compare our data with a very recent experiment performed by Beyer *et al.* at Helmholtz-Zentrum Dresden-Rossendorf (HZDR) using the photoneutron source the neutron time-of-flight facility at the Electron Linac for beams with high Brilliance and low Emittance (nELBE) using an HPGe detector positioned at 125° [12].

*alnegret@tandem.nipne.ro

The latest evaluations of the neutron inelastic cross sections on ^{56}Fe are generally based on older, very detailed evaluations. Evaluated Nuclear Data File (ENDF)/B-VII.1 below 20 MeV is based on ENDF/B-VI.1 [13] while Joint Evaluated Fission and Fusion File (JEFF) 3.1.2 is based on the older Evaluated Fission and Fusion File 3.0 database, which is obtained by combining the smooth data from an evaluation by Pronyaev *et al.* [14] with the fluctuations from a measurement performed at the Institute for Reference Materials and Measurements (EC-JRC-IRMM) by Dupont *et al.* [15].

The next section of this article describes the experimental procedure emphasizing the various consistency checks we performed. The third section briefly presents the theoretical calculations performed with the TALYS 1.6 reaction code while the fourth one discusses in detail the results. The last section is dedicated to a few concluding remarks.

II. EXPERIMENTAL PROCEDURE

The experimental approach used in the present measurement is based on the detection of the γ rays emitted following the inelastic scattering of neutrons on the target. The time-of-flight (ToF) technique is employed to determine the energy of the incident neutrons and the γ transitions are identified based on their energy using HPGe detectors. This allows the determination, for each value of the neutron energy, of the γ production cross section. Further, the method uses the level scheme from an external source [16] to compute the total inelastic cross section as a sum of the γ production cross sections decaying to the ground state. Also, level cross sections are determined as the difference between the cross sections of the transitions depopulating the level and those feeding it. The authors of Ref. [17] described this technique in detail.

A. Experimental setup

The white neutron source Geel Linear Accelerator (GELINA) produces pulses of neutrons of less than 1 ns with a repetition rate of 800 Hz [18,19]. The direct neutron flux is significant in the energy range from 0.1 to about 18 MeV. A 198.68-m flight path was used. A ^{10}B filter was employed to eliminate the overlap neutrons and a ^{238}U filter was used to limit the intensity of the γ flash (γ rays produced by GELINA together with each neutron burst). At the position of the sample the beam diameter was 6.1 cm.

The Gamma Array for Inelastic Neutron Scattering (GAINS) spectrometer is installed in an experimental cabin located 200 m away from the neutron source [20,21]. It consisted of eight high-efficiency HPGe detectors placed at 110° and 150° with respect to the incoming beam. These angles, the nodes of the fourth degree Legendre polynomial, allow a precise angle integration for γ transitions with multipolarity up to three [17].

The eight detectors are readout by an acquisition system based on four DC440 digitizers produced by Acqiris, with 12 bits amplitude resolution (4096 channels) and a sampling frequency of 420 Msamples/s (2.38 ns/sample). These characteristics are sufficient for the energy and time resolution achievable with HPGe detectors. Each digitizer accommodates two detectors and a common trigger. To limit the counting rate, the trigger signal is issued only when an event takes place in the time region of interest. Each of the two digitizers fit in an Acqiris compact PCI crate that is connected to a PC. The DC440 card has no on-board processing capabilities. The waveforms are transferred to PCs where the acquisition software performs the online processing and stores time-amplitude list files. The algorithms used in the acquisition and their performances were discussed in Ref. [22]. Both the time resolution (8 ns for 1-MeV neutrons) and the energy resolution ($<$2.5 keV for 1-MeV γ rays) are comparable to those obtained with conventional Nuclear Instrumentation Module (NIM) electronics.

The beam is monitored by a fission chamber with ^{235}U placed in the beam in the cabin at 200 m [23]. All absolute values measured are therefore based on the fission cross section of ^{235}U [24].

The sample consisted of ^{nat}Fe plates (99.5 % purity) with a thickness of 1 mm and diameter of 80 mm. The composition of the iron plates was checked by a transmission measurement performed at Institute for Reference Materials and Measurements (IRMM). Most of the data were taken with three plates bound together. The results shown in the present article are obtained from the analysis of these data. However, to check the consistency of the method, additional data-taking runs were performed for sample thicknesses of 1 and of 4 mm. The results from the three measurements are shown together with other consistency checks in Sec. II E.

B. Data analysis algorithm

The method used in this work was extensively employed in the past to produce high-quality cross-section data [25–31]. We present here only a very short summary of the analysis technique.

The offline analysis of the experimental data includes the processing of the time-amplitude list files from the germanium detectors and from the fission chamber, but also Monte Carlo *N*-particle transport code (MCNP)[32] simulations used to determine the corrections for neutron multiple scattering and γ absorption processes in the sample.

The eight HPGe detectors produce independent time-amplitude list files. For each event the time information is related to the energy of the scattered neutron and the amplitude is used do identify the γ transition by energy. An MCNP simulation is used to determine the correction factor for multiple scatterings of the neutrons in the target.

The detectors are efficiency calibrated using a point-like ^{152}Eu source. A simulation of the detectors is employed to fit the experimental calibration data for the point-like radioactive source and then to correct for the finite size of the sample [33]. Figure 1 displays the experimental efficiency for one of the detectors together with the MCNP simulation of the point-like and of the extended sources.

Based on the differential cross section at 110° and 150° the angle-integrated cross section can be calculated precisely for transitions of multipolarities up to three. These are the γ production cross sections and they represent the primary experimental result. Further, using the evaluated level scheme [16]

we deduce the total inelastic cross section and various level cross sections. We should note that only a limited number of γ transitions are observed, mainly due to statistical limitations. The level cross section can be calculated when at least one γ transition is observed from a level. The total cross section determined with the present method is precise up to the energy of the last observed level. Beyond this energy it represents only a lower limit of the real inelastic cross section. However, this limit is very close to the real value because most of the γ decay of ^{56}Fe proceeds through the first excited level (846.8 keV, $J^{\pi} = 2^{+}$) and the decay of this level is clearly observed. Similarly, the calculated level cross sections are precise only up to the energy of the last observed level. Beyond this energy they represent upper limits because the possible feeding from higher levels or from the continuum is not observed.

C. Data uncertainties and correlations

The experimental results obtained via this procedure are influenced by a few sources of uncertainty. We distinguish several sources of uncertainty that introduce correlations between various cross sections determined in our experiment. A significant contribution to this *correlated* uncertainty comes from the activity of the source used for efficiency calibration of the HPGe detectors: 0.7%. This is common for all detectors, unlike other sources of uncertainty (e.g., the peak integration procedure or the inaccurate reproduction of the experimental efficiency of the HPGe detectors by the simulation—see Fig. 1). The statistical uncertainty of the HPGe data is of the order of 2% for each detector for the strongest neutron energy channels. This is reduced by the fact that we use eight detectors. Further, if the statistical uncertainty remains too high, we group a few time channels adding the statistics and sacrificing time resolution. The beam monitoring with the fission chamber adds another *correlated* uncertainty of 1.5%. The fission chamber has a rather poor efficiency and a special procedure is applied to reduce the statistical uncertainty to this value. Considering all sources of error, we conclude that the cross sections we

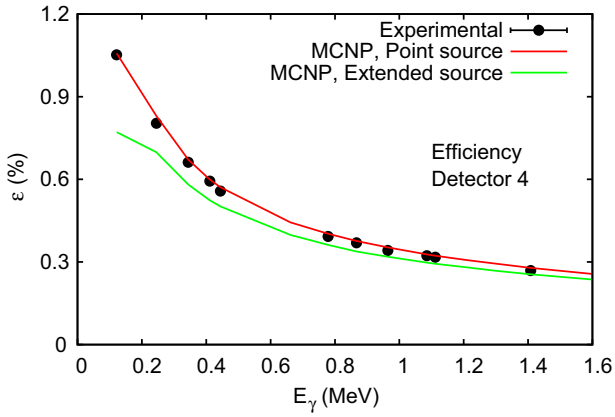

FIG. 1. (Color online) Efficiency of one of the HPGe detectors. The black points represent the experimentally measured efficiency using a calibrated ^{152}Eu source. The red line shows the result of an MCNP simulation of a point-like source and the green line display the results of the MCNP simulation for an extended ^{56}Fe sample.

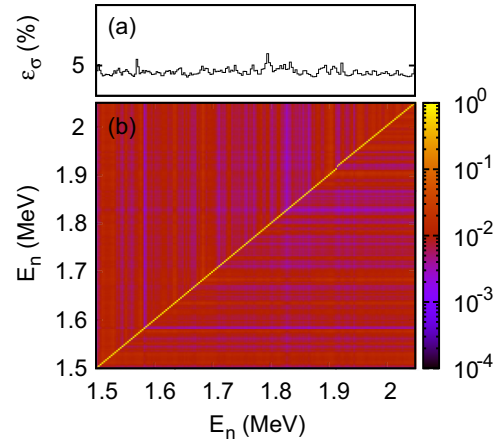

FIG. 2. (Color online) Relative uncertainties and correlation matrix for the total inelastic cross section.

deduce for the strongest channels have an uncertainty of the order of 5–6%, analytically calculated using the well-known uncertainty propagation formula. This is visible in Figs. 2(a) and 11(a) where the uncertainty of the total inelastic cross section is displayed: in the energy region where the cross section has large values the uncertainty is indeed between 5% and 6%.

A Monte Carlo procedure was recently developed to asses also the correlations introduced by the current analysis algorithm. As described also in Refs. [21,34], this approach is based on the fact that the covariance of two variables that are repeatedly measured n times can be estimated as

$$\mathrm{cov}(x,y) = \frac{1}{n-1}\sum_{i=1}^{n}(x_i - \bar{x})(y_i - \bar{y}). \qquad (1)$$

As the repetition of our measurement for a large number of times is not feasible, we only *simulated* this by varying the most important observables of our experimental procedure in a consistent way. A more technical and detailed description of these variations is given in Ref. [34]. We limited our analysis to the variation of the HPGe and FC yields and efficiencies, taking care that each variation follows the correct distribution and is performed obeying the existing experimental correlations. The whole data analysis was repeated each time obtaining $n =$ 25 000 sets of results. Equation (1) was finally applied allowing the calculation of the covariance for any pair of cross-section values.

Our covariance generation procedure, although using a powerful, very general approach, has the significant limitation of revealing mainly the correlations introduced by the analysis (even if we try to account also for the most obvious experimental correlations like those introduced by the use of the same γ source for the calibration of the HPGe detectors). Also, as previously said, our analysis regarded only the most important observables.

Figure 2 shows a limited area of the correlation matrix $[\mathrm{cor}(x,y) = \mathrm{cov}(x,y)/(\sigma_x\sigma_y)]$ among total inelastic cross-section values together with the relative uncertainties for the same energy range. We note that, besides the diagonal

elements that are equal to 1 by definition, the other correlation values resulting from this procedure are one to three orders of magnitude smaller.

D. Experimental particularities and challenges

A few particularities make the present experiment not trivial. The main gamma transition in ^{56}Fe has the energy $E_\gamma = 846.8$ keV and it accounts for more than 95% of the total inelastic cross section for the entire neutron energy range. The precise determination of the γ production cross section for this transition may be influenced by three possible sources of background.

(1) The first γ transition in ^{27}Al has $E_\gamma = 843.7$ keV. The neutrons scattered on Fe or air could undergo an inelastic scattering on the ^{27}Al surrounding the Ge crystals producing the 843.7-keV γ ray. The presence of the aluminum in the structure of the HPGe detectors cannot be avoided. The design of GAINS tries to limit any additional quantity of aluminum in close vicinity of the sample. The detectors are held by their cryogenic vessels and only the aluminum container of the crystal is very close to the sample.

(2) A second source of γ background in this energy region is due to the germanium crystal itself. The inelastic excitation of ^{72}Ge produces a γ ray of 834.01 keV. This energy is detected together with the recoil energy of the ^{72}Ge nucleus resulting in a specific triangular shape in the spectrum of any HPGe detector exposed to a neutron flux with various energies [35].

(3) Finally, one should also consider the small amount of ^{56}Fe that exists in the structure of the detectors.

To check the level of the background in the region of interest we irradiated an Ni sample under the same conditions as those for iron. Figure 3 shows the two γ spectra collected by one of the detectors scaled to compensate for the different acquisition time and sample thickness. As the spectrum from Ni shows no structure around 846.7 keV, we could estimate the background contributions for that γ energy range. The germanium contribution is weakly visible and it has a smooth behavior under the peak of interest. The contribution from a possible aluminum or iron contamination is negligible.

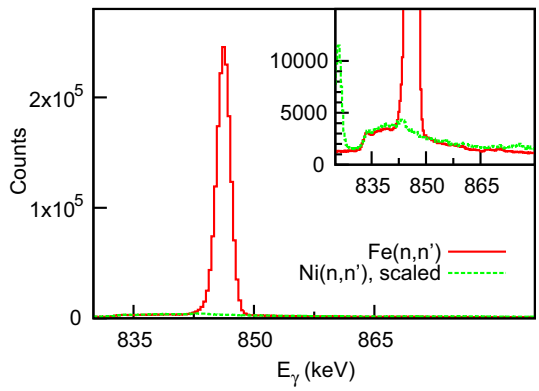

FIG. 3. (Color online) Comparison of the spectrum obtained with the iron and with a nickel sample for the energy region around the main γ line from ^{56}Fe. The Ni data were scaled to compensate for a different target thickness and acquisition time.

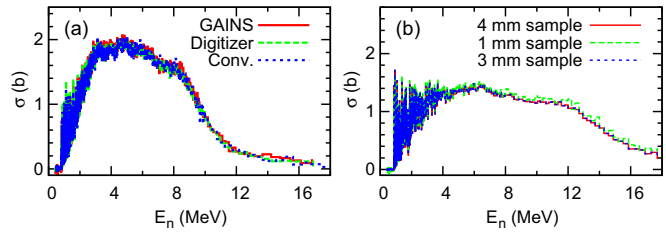

FIG. 4. (Color online) (a): Comparison of the cross section of the strongest γ transition in ^{206}Pb obtained with various setups. "GAINS" denotes the result obtained with the present setup. The curves named "Digitizer" and "Conventional" were obtained with the previous setup (only 4 HPGe detectors in a horizontal plane) readout by a conventional and a digitized acquisition, respectively. (b): The γ production cross section of the strongest transition in ^{56}Fe obtained with various sample thicknesses.

E. Consistency checks

The present experiment represents the first measurement performed with the GAINS array [20]. Therefore a number of checks were performed to make sure that the data are consistent and reliable. Figure 4 shows the two most important of these verifications.

An additional data taking run was performed with a ^{206}Pb sample. Figure 4(a) compares the cross section of the strongest γ ray from the ^{206}Pb$(n, n\gamma)$ reaction. The curves labeled "Digitizer" and "Conventional" represent the results of two previous measurements. The curve labeled "GAINS" resulted from the dedicated run during the present experiment. The perfect overlap of the three results represented the ultimate test of the new setup.

Figure 4(b) shows three results obtained during the present measurement using samples with different thicknesses (see Sec. II A). The agreement of the three curves is a proof that the analysis procedure that corrects for the extended size of the sample is valid and produces consistent results.

III. THEORETICAL CALCULATIONS

The evaluated level scheme of ^{56}Fe from Ref. [16] is shown in Tables I and II. The structure of ^{56}Fe at low excitation energies is described by two proton-holes in the $1f7/2$ orbital and two neutrons on the $2p3/2$ orbital. The threshold for the inelastic channel is 861.9 keV. Immediately after the threshold the inelastic cross section is dominated by the compound-nucleus mechanism. As the energy of the incoming neutron increases, the direct and the preequilibrium reaction mechanisms play a more significant role while the various inelastic channels open. The $(n, 2n)$ channel opens at 11.4 MeV.

Our results are compared to the reaction calculations preformed with the version 1.6 of the TALYS code [36,37].

TABLE I. List of levels and γ transitions in ^{56}Fe below the excitation energy of equal to 4 MeV, according to the latest evaluation [16]. Production cross sections for the levels and for the γ transitions emphasized with bold characters were determined in the present work and are presented below.

E_L^i (keV)	J_i^π	E_γ (keV)	Branching ratio (%)	E_L^f (keV)	J_f^π
846.8	2^+	**846.8**	100	0	0^+
2085.1	4^+	**1238.3**	100(2)	846.8	2^+
2657.6	2^+	**1810.8**	100.0(3)	846.8	2^+
		2657.5	3.1(3)	0	0^+
2941.5	0^+	**2094.9**	100	846.8	2^+
2960.0	2^+	**2113.1**	100(2)	846.8	2^+
		2959.9	2.16(8)	0	0^+
3076.2	(3^-)	991.5	47(13)	2085.1	4^+
		2229	100(13)	846.8	2^+
3120.1	(1^+)	462	<1.05	2657.6	2^+
		2273.2	100.0(7)	846.8	2^+
		3120	4.82(7)	0	0^+
3123.0	4^+	**1037.8**	100.0(4)	2085.1	4^+
		2276.1	0.85(5)	846.8	2^+
3370.0	2^+	**2523.1**	100.0(9)	846.8	2^+
		3369.8	17(1)	0	0^+
3388.6	6^+	265.5	1.3(3)	3123.0	4^+
		1303.4	100(4)	2085.1	4^+
3445.3	3^+	787.7	1.83(2)	2657.6	2^+
		1360.2	25.63(8)	2085.1	4^+
		2598.5	100.0(4)	846.8	2^+
3448.4	1^+	790	<0.7	2657.6	2^+
		2601	33(3)	846.8	2^+
		3448	100(3)	0	0^+
3600.2	$(1,2^+)$	942	<2.4	2657.6	2^+
		1515	<2.4	2085.1	4^+
		2753	20(4)	846.8	2^+
		3600	100(4)	0	0^+
3605.7	2^+	948	14.2(20)	2657.6	2^+
		1521	<1.4	2085.1	4^+
		2759	100(5)	846.8	2^+
		3606	56(5)	0	0^+
3610.2	$0(^+)$	952	<1.5	2657.6	2^+
		1525	<0.7	2085.1	4^+
		2763	100.0	846.8	2^+
		3610	<7.0	0	0^+
3744.1	2^+	2897	100	846.8	2^+
3755.6	6^+	367.0	22(1)	3388.6	6^+
		632.6	$\leqslant$2	3123.0	4^+
		1670.8	100(4)	2085.1	4^+
3829.8	2^+	1172	58(10)	2657.6	2^+
		2983	100(10)	846.8	2^+
		3830	35(4)	0	0^+
3856.5	3^+	411.1	0.17(1)	3445.3	3^+
		486.6	0.38(2)	3370.0	2^+
		733.5	1.24(3)	3123.0	4^+
		896.5	0.46(1)	2960.0	2^+
		1198.9	0.28(2)	2657.6	2^+
		1771.4	100.0(3)	2085.1	4^+
		3009.6	6.42(14)	846.8	2^+

TABLE II. Same as Table I for excitation energies higher than 4 MeV.

E_L^i (keV)	J_i^π	E_γ (keV)	Branching ratio (%)	E_L^f (keV)	J_f^π
4048.9	3^+	1088.9	1.7(1)	2960.0	2^+
		1963.7	22.0(1)	2085.1	4^+
		3202.0	100.0(4)	846.8	2^+
4085.9	$(1,2^+)$	3239	100(8)	846.8	2^+
		4086	33(8)	0	0^+
4100.4	4^+	655.0	0.45(10)	3445.3	3^+
		977.4	18.05(9)	3123.0	4^+
		1140.4	1.68(5)	2960.0	2^+
		1442.7	2.29(5)	2657.6	2^+
		2015.2	38.3(5)	2085.1	4^+
		3253.5	100.0(4)	846.8	2^+
4119.9	3^+	263.4	0.30(3)	3856.5	3^+
		674.6	0.45(6)	3445.3	3^+
		996.9	1.50(8)	3123.0	4^+
		1159.9	1.14(4)	2960.0	2^+
		1462.3	1.00(1)	2657.6	2^+
		2034.8	100.0(4)	2085.1	4^+
		3273.1	23.97(12)	846.8	2^+
4298.1	4^+	852.7	2.18(13)	3445.3	3^+
		1175.1	100.0(4)	3123.0	4^+
		1640.5	2.76(9)	2657.6	2^+
		2212.9	17.1(2)	2085.1	4^+
		3451.2	41.9(3)	846.8	2^+
4302.0	0^+	3455.0	100	846.8	2^+
4320	2^+				
4394.9	3^+	1271.9	10.3(4)	3123.0	4^+
		3548.1	100.0(8)	846.8	2^+
4401.3	2^+	955.8	46(3)	3445.3	3^+
		1031	<2.0	3370.0	2^+
		1441	11.7(23)	2960.0	2^+
		1459.3	7.7	2941.5	0^+
		2316	<6.3	2085.1	4^+
		3554.2	100(3)	846.8	2^+
4447.7		3600.8	100	846.8	2^+
4458.5	4^+	**1335.4**	100.0(13)	3123.0	4^+
		2373.2	64(5)	2085.1	4^+
		3611.5	6.8(3)	846.8	2^+
4509.6	3^-	754.4	<21	3755.6	6^+
		1064.6	6(4)	3445.3	3^+
		1139.7	39(17)	3370.0	2^+
		1386.3	28(15)	3123.0	4^+
		1852.1	100	2657.6	2^+
		2424.9	20(8)	2085.1	4^+
		3662.7	98(18)	846.8	2^+

A. TALYS reaction code

TALYS is a well known reaction software built for two purposes.

First, it is a nuclear physics tool used for the analysis of nuclear-reaction experiments. A proper theoretical understanding of the experimental data can provide valuable insights in the characteristics of the interaction between particles and nuclei. Further, a so-called "microscopic" approach can be used in TALYS, which means that some parameters (like

the level density) are deduced from microscopic models. A good overlap of these calculations with the experimental data represents a verification of the range where the microscopic models are valid.

Second, after a proper validation, TALYS can be transformed into a nuclear data tool used to generate nuclear data that are hardly measurable. Using a set of fine-tuned parameters means in reality that the new data are interpolated and extrapolated from the existing experimental information.

The code integrates ECIS-06 [38] as a routine used for optical model and for coupled-channels calculations.

The main strength of TALYS resides in its completeness: It implements in a unified and modern approach various reaction mechanisms (direct, compound, multistep, and fission) and can be used for a very wide range of energies (1 keV–200 MeV) and target nuclei ($A = 12$–339). Therefore the code has a remarkable predictive power. Based on a very reduced number of input parameters it can generate acceptable cross sections by making reasonable documented choices.

B. TALYS 1.6 Calculations for ^{56}Fe

γ production, level production, and total inelastic cross sections were computed using TALYS.

To check the predictive power of TALYS we performed, first of all, calculations using exclusively default parameters. A second calculation was made using parameters determined from microscopic models.

The optical model used in the default TALYS calculation is based on the Koning-Delaroche potential [39] while the microscopic calculation uses the Lane-consistent potential of Bauge *et al.* [40]. Both were adjusted to the neutron total cross-section data for ^{56}Fe and neutron differential scattering data in the energy range from 4 to 26 MeV [39,40]. Figure 5 compares the calculated total cross sections for $n + ^{56}$ Fe with the experimental data of Cornelis *et al.* [41] and Harvey *et al.* [42]. To facilitate the comparison, the experimental data were averaged over 100-keV energy bins. The microscopic calculation and default calculation differ significantly in trend below 5 MeV and in magnitude up to 15% from 5 to 15 MeV. The microscopic calculation is in good agreement with the experiment below 2.5 MeV while the default calculation using the Koning-Delaroche potential reproduces very well the empirical data above 2.5 MeV.

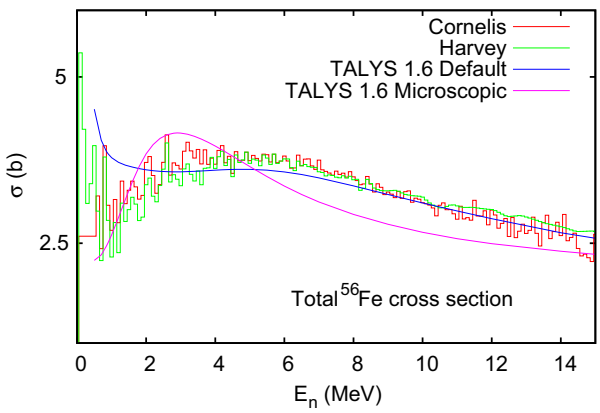

FIG. 5. (Color online) Total neutron cross section on ^{56}Fe: Comparison of the TALYS 1.6 calculations using the default and the microscopic approach with experimental data from Refs. [41,42].

The default and microscopic calculations use 20 discrete levels from the Reference Input Parameter Library (RIPL-3) database [43] with a few modifications. The level energies and decay branches are consistent with the nuclear structure evaluation of Ref. [16] up to the 18th excited level ($E_L =$ 3759.6 keV). This level for which no decay branches were measured was assigned $J^\pi = 1^+$ and decay modes to the ground state and the first excited state with equal probability. The tentative spin-parity assignments for the sixth [$E_L =$ 3076.2 keV, $J^\pi = (3^-)$] and the seventh [$E_L = 3120.1$ keV, $J^\pi = (1^+)$] excited levels were adopted in the calculation and the 13th excited level ($E_L = 3600.2$ keV, $J^\pi = (1,2^+)$ in Ref. [16]) was assigned spin and parity 2^+.

The default calculation uses the Gilbert-Cameron level density description with parameters adjusted to match the discrete levels and s-wave spacings (D0) where available. The parameters are otherwise taken from systematics [44]. For ^{56}Fe the adjustment involves levels 8 to 15 and the s-wave level spacing of 25 400 eV. The microscopic calculation with level densities from Ref. [45] is shown without the adjustment to discrete levels and D0. However, we checked the adjusted level densities proposed by Ref. [45] and found no significant impact on the calculated cross sections.

For the modeling of the γ-decay the default calculation uses the Kopecky-Uhl generalized Lorentzian γ-strength functions [46] while the microscopic calculation uses the strength functions of Ref. [47]. The former reproduce the available data on the giant resonance photoabsorption cross section and are adjusted to the mean γ-decay width in the neutron incident energy range below 100 keV. The microscopic strength functions were not adjusted to data for the Fe or nearby nuclei. Further details about the calculations may be found in Refs. [37,48].

We emphasize that for both calculations none of the parameters were fitted on the present data. However, we note that previous experiments and in particular the total cross section and the elastic scattering angular distributions on ^{56}Fe were used to adjust some of the default parameters.

IV. RESULTS AND DISCUSSION

As mentioned in Sec. II, the results of our experiment consists of γ production cross sections, level cross sections, and the total inelastic cross section. We will further present and discuss in detail each of these results.

A. γ production cross sections

Twenty γ rays were sufficiently intense so that the γ production cross section could be determined. These γ transitions are emphasized in Tables I and II [16].

Figure 6 displays the the production cross section of the 846.8-keV γ ray, which represents the most important transition, collecting most of the inelastic strength. Our

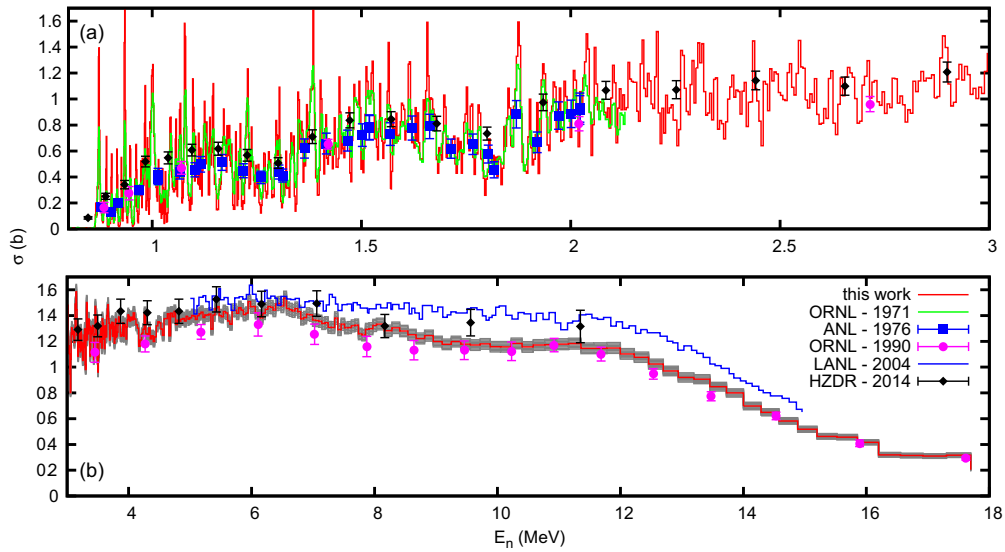

FIG. 6. (Color online) Integral production cross section for the 846.8 keV γ ray compared to several previous measurements. ORNL-1971, ANL-1976, ORNL-1990, LANL-2004, and HZDR-2014 label the results presented in Refs. [8–12], respectively. The gray band from panel (b) represents the uncertainties of our measurement.

results are compared to those of Perey *et al.* obtained at ORNL in 1971 [8], Smith (ANL-1976) [9], Dickens *et al.* (ORNL-1990) [10], Nelson *et al.* (LANL-2004) [11], and the very recent measurement of Beyer *et al.* (HZDR-2014) [12]. Figures 7 and 8 compare our results with those obtained by Nelson *et al.* [11] and Dickens *et al.* [10], but also with TALYS calculations. We note that, for a proper comparison, the ANL-1976 and the LANL-2004 data where ^{nat}Fe targets were used were scaled to account for the isotopic abundance of ^{56}Fe. Generally, our data have higher resolutions than the previous experiments. A good overall agreement is found both with the previous data and with TALYS. However, certain discrepancies are important.

For the strongest transition at 846.8 keV our result is slightly higher than the measurement performed at ORNL for neutron energies below 8 MeV. We agree perfectly with the LANL result for incident neutron energies around 6.5 MeV while a difference appears above this energy. It is difficult to directly compare various experiments at low neutron energies when the resolution is very different [Fig. 6(a)]. We note that, after a proper rebining of our data, our result is in very good agreement with the recent set from HZDR.

We note that the 846.8-keV γ ray can also be produced in the ^{57}Fe$(n, 2n\gamma)^{56}$Fe reaction by neutrons with $E_n > 8.5$ MeV. A separate measurement performed using an enriched ^{57}Fe sample allowed us to estimate this contribution: The production cross section of the 846.8-keV γ ray in the ^{57}Fe$(n, 2n\gamma)^{56}$Fe reaction reaches a maximum value of about 0.9 b for $E_n \approx 15$ MeV [21]. Considering the abundance of ^{57}Fe in our isotopically natural sample of 2.12% we conclude that the contribution coming from ^{57}Fe$(n, 2n\gamma)^{56}$Fe is at the level of maximum 19 mb around $E_n \approx 15$ MeV, below our uncertainties in that energy range. The correction for the $(n, 2n)$ contribution was therefore not applied the the 846.8-keV γ production cross section.

The γ production cross sections for the transitions with $E_\gamma = 2094.9$, 2273.2, and 1303.4 keV, are in very good agreement both with the ORNL result and the default TALYS calculations. In a few cases ($E_\gamma = 1810.8$, 1037.8, and 1670.8 keV) our result is in good agreement with the ORNL data while TALYS fails to reproduce the experiment.

It is surprising that the microscopic approach from TALYS does not produce improved results. Moreover, the microscopic calculation is clearly worse than the default calculation for the transitions with $E_\gamma = 1238.3$ and 1303.4 keV. We note that in the case of ^{206}Pb the agreement between the experiment and TALYS was significantly improved in the microscopic approach. This could be interpreted as a sign that the microscopic representation of ^{56}Fe is more difficult than the one of ^{206}Pb, which is understandable taking into account the more complicated structure of the nucleus.

Finally, we observe that for the majority of γ transitions the agreement with TALYS is better for 1–2 MeV above the threshold. This suggests again that the nuclear structure or the population mechanism of ^{56}Fe is not well accounted for in this type of calculation, whether based on semi-empirical or on semimicroscopic models.

B. $(n, 2n\gamma)$ γ production cross sections

The γ production cross sections for six transitions from the ^{56}Fe$(n, 2n\gamma)^{55}$Fe reaction were determined. They are listed in Table III. The neutron separation energy in ^{56}Fe is $S_n = 11.2$ MeV. Figure 9 compares the experimental result to TALYS 1.6 estimates. The agreement is reasonable in all cases for the limited neutron energy range where we could determine the cross section; the default and the microscopic TALYS calculation reproduce the data equally well. However, the low-lying discrete levels seem to be better described than the higher levels, indicating a possible difficulty in modeling the continuum.

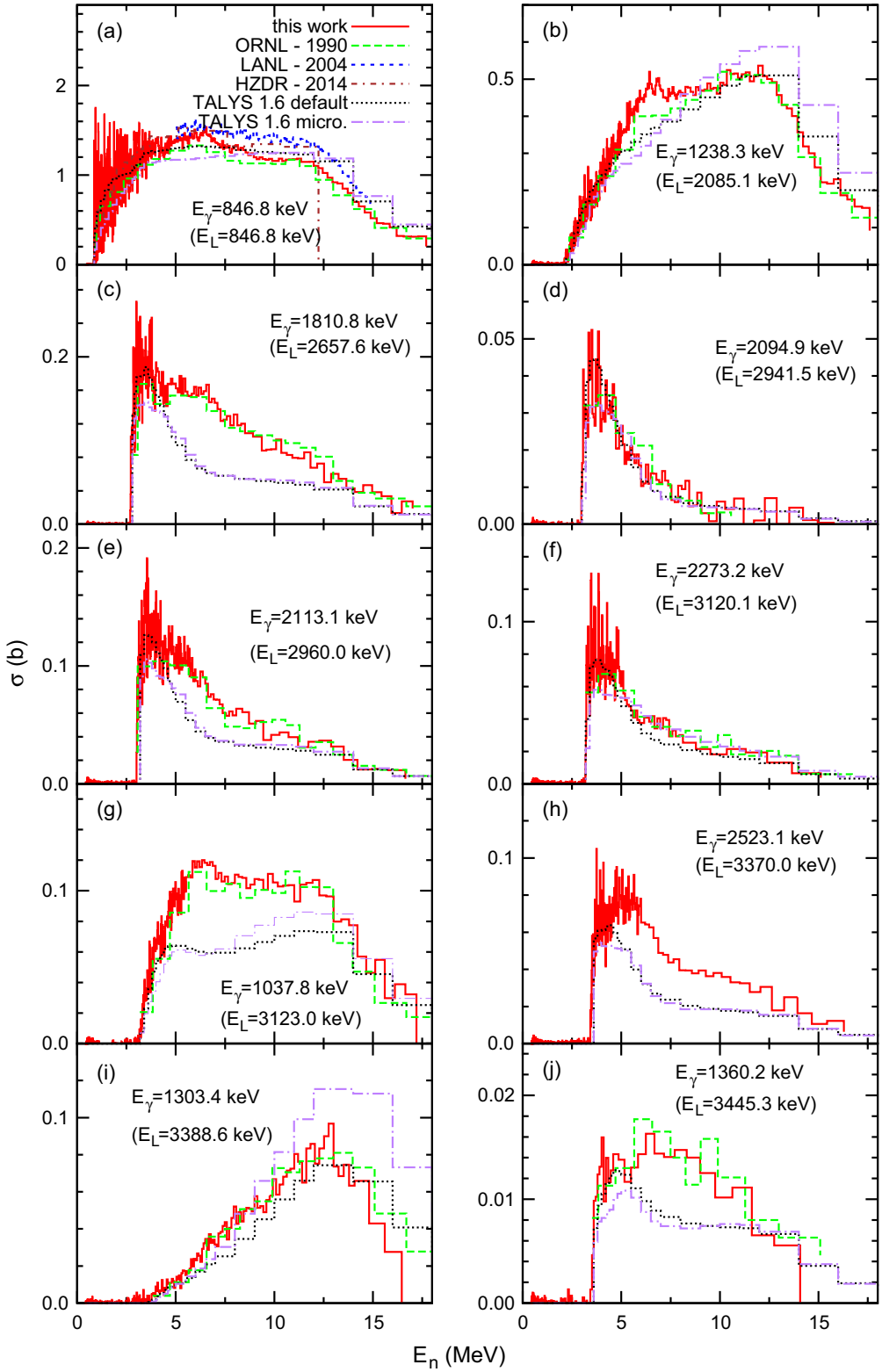

FIG. 7. (Color online) Integral production cross section for the γ rays from the ^{56}Fe(n, $n'\gamma$)^{56}Fe reaction.

C. Angular distribution of the 846.8-keV γ transition

As described in Sec. II A the current measurement was performed using HPGe detectors placed at $\theta = 110^\circ$ and 150° with regard to the incoming neutron beam. Therefore a complete angular distribution of the 846.8-keV γ transition cannot be built. However, our data allows the determination of the ratio between the differential cross section at 110° and 150° as a function of the neutron energy E_n.

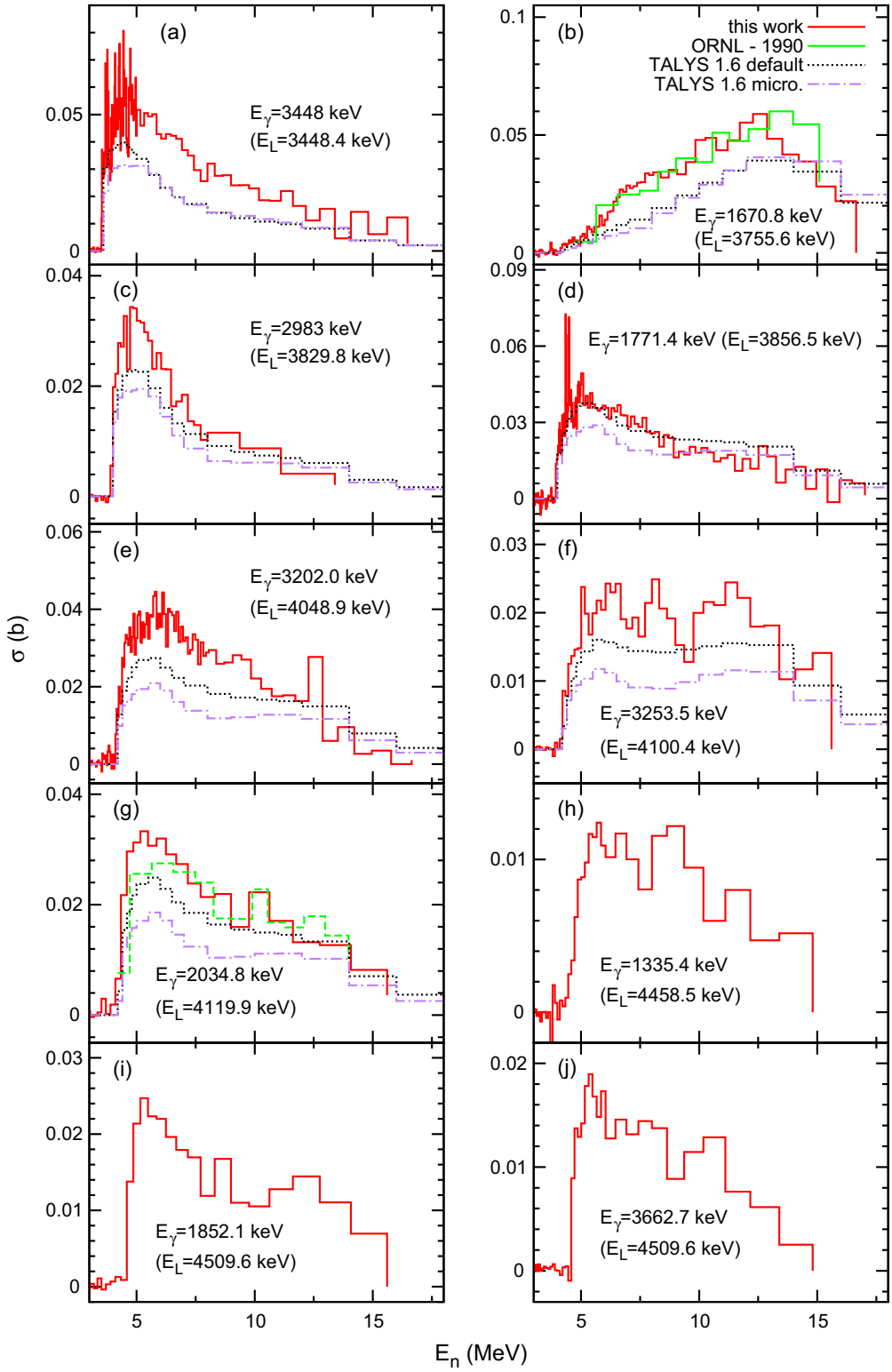

FIG. 8. (Color online) Integral production cross section for the γ rays from the ^{56}Fe$(n, n'\gamma)^{56}$Fe reaction.

A detailed angular distribution of the 846.8-keV γ transition was measured by Smith at Argonne National Laboratory (ANL) for 11 values of E_n with a neutron energy resolution of 65 keV [9]. The authors fit their angular distributions using the following well-known formula

$$\frac{d\sigma}{d\omega}(E_n) = \frac{\sigma(E_n)}{4\pi}[1 + w_2(E_n)P_2(\cos\theta) + w_4(E_n)P_4(\cos\theta)] \quad (2)$$

TABLE III. Observed γ rays from the ^{56}Fe$(n, 2n\gamma)^{55}$Fe reaction. The $(n, 2n)$ reaction threshold is 11.4 MeV and the ground state of ^{55}Fe has $J^\pi = 3/2^-$.

Level energy (keV)	J^π	γ energy (keV)
411.4	$1/2^-$	411.9
931.3	$5/2^-$	931.3
1316.5	$7/2^-$	1316.4
1408.5	$7/2^-$	477.2
2211.9	$9/2^-$	803.4
2539.1	$11/2^-$	1222.5

and provided in their report the values of the $w_i(E_n)$ coefficients of the Legendre polynomials $P_i(\cos\theta)$. Based on these values we can compare the $\frac{d\sigma}{d\omega}(E_n)$ ratios measured in our experiment to those measured at ANL. Figure 10 shows this comparison displaying a good overlap of our data with those from ANL. However, we note that this reflects only the good agreement of the $w_2(E_n)$ coefficients determined in the two measurements as our choice of scattering angles as the nodes of $P_4(\cos\theta)$ does not allow any statement with regard to $w_4(E_n)$.

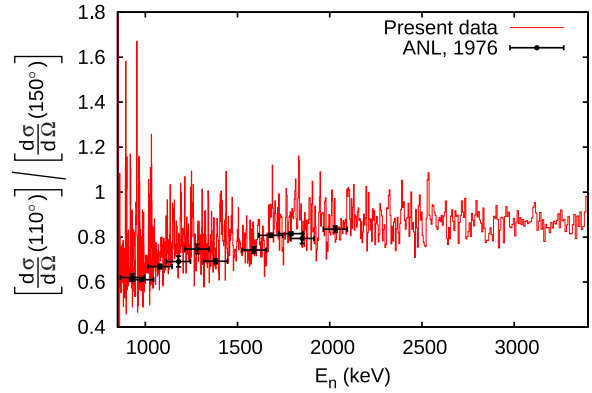

FIG. 10. (Color online) The ratio between the differential cross section of the 846.8-keV γ ray measured at 110° and 150° compared to the values calculated based on the angular distributions from Ref. [9].

D. Total inelastic and level cross sections

The total neutron inelastic cross section and the level production cross sections for ten excited states in ^{56}Fe were calculated starting from the γ production cross sections. The level sequence, the placement of the γ transitions, and the branching ratios were taken from the latest nuclear

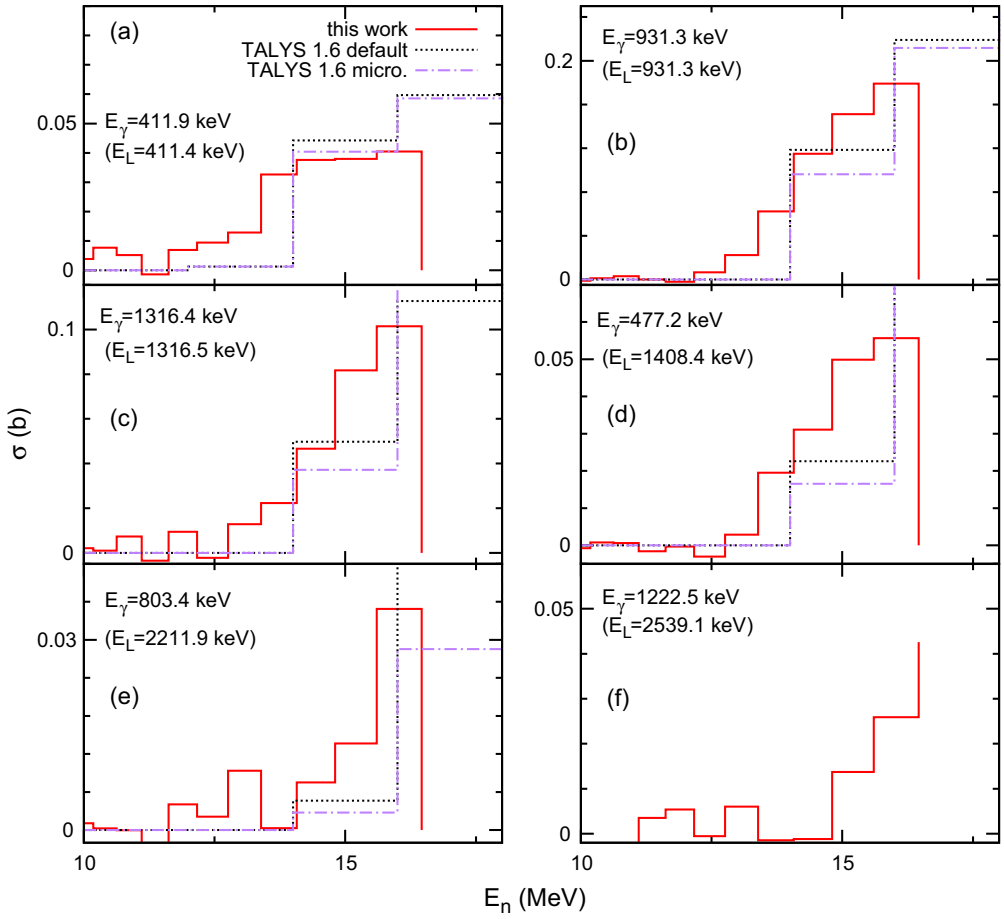

FIG. 9. (Color online) Integral production cross section for the γ rays from the ^{56}Fe$(n, 2n\gamma)^{55}$Fe reaction.

TABLE IV. Formulas used for the calculation of the total inelastic and level cross sections as a function of the measured γ production cross sections and the neutron energy ranges where they apply.

Level/Total inelastic cross section	Formula	Range (keV)
$\sigma^{\text{Total inelastic}}$	$1.000\sigma_\gamma^{847} + 0.031\sigma_\gamma^{1811} + 0.022\sigma_\gamma^{2113} + 0.048\sigma_\gamma^{2273} + 0.170\sigma_\gamma^{2523} + 1.000\sigma_\gamma^{3448} + 0.350\sigma_\gamma^{2983}$	862–4500
$\sigma_L^{846.8}$	$1.000\sigma_\gamma^{847} - 1.000\sigma_\gamma^{1238} - 1.000\sigma_\gamma^{1811} - 1.000\sigma_\gamma^{2095} - 1.000\sigma_\gamma^{2113} - 1.000\sigma_\gamma^{2273}$ $-0.009\sigma_\gamma^{1038} - 1.000\sigma_\gamma^{2523} - 3.902\sigma_\gamma^{1360} - 0.330\sigma_\gamma^{3448} - 1.000\sigma_\gamma^{2983} - 0.064\sigma_\gamma^{1771}$ $-1.000\sigma_\gamma^{3202} - 1.000\sigma_\gamma^{3254} - 0.240\sigma_\gamma^{2035} - 0.068\sigma_\gamma^{1335} - 1.000\sigma_\gamma^{3663}$	862–4500
$\sigma_L^{2085.1}$	$1.000\sigma_\gamma^{1238} - 1.000\sigma_\gamma^{1038} - 1.000\sigma_\gamma^{1303} - 1.000\sigma_\gamma^{1360} - 1.000\sigma_\gamma^{1671} - 1.000\sigma_\gamma^{1771}$ $-0.220\sigma_\gamma^{3202} - 0.383\sigma_\gamma^{3254} - 1.000\sigma_\gamma^{2035} - 0.640\sigma_\gamma^{1335} - 0.100\sigma_\gamma^{1852}$	2122–4500
$\sigma_L^{2657.6}$	$1.031\sigma_\gamma^{1811} - 0.006\sigma_\gamma^{2273} - 0.071\sigma_\gamma^{1360} - 0.004\sigma_\gamma^{3448} - 0.580\sigma_\gamma^{2983} - 0.003\sigma_\gamma^{1771}$ $-0.023\sigma_\gamma^{3254} - 0.010\sigma_\gamma^{2035} - 1.000\sigma_\gamma^{1852}$	2705–4500
$\sigma_L^{2941.5}$	$1.000\sigma_\gamma^{2095}$	2994–4500
$\sigma_L^{2960.0}$	$1.022\sigma_\gamma^{2113} - 0.005\sigma_\gamma^{1771} - 0.017\sigma_\gamma^{3202} - 0.017\sigma_\gamma^{3254} - 0.011\sigma_\gamma^{2035}$	3013–4500
$\sigma_L^{3120.1}$	$1.053\sigma_\gamma^{2273}$	3176–4500
$\sigma_L^{3123.0}$	$1.009\sigma_\gamma^{1038} - 0.013\sigma_\gamma^{1303} - 0.010\sigma_\gamma^{1671} - 0.012\sigma_\gamma^{1771} - 0.181\sigma_\gamma^{3254} - 0.015\sigma_\gamma^{2035}$ $-1.000\sigma_\gamma^{1335} - 0.280\sigma_\gamma^{1852}$	3179–4500
$\sigma_L^{3370.0}$	$1.170\sigma_\gamma^{2523} - 0.004\sigma_\gamma^{1771} - 0.390\sigma_\gamma^{1852}$	3430–4500
$\sigma_L^{3388.6}$	$1.013\sigma_\gamma^{1303} - 0.220\sigma_\gamma^{1671}$	3449–4500
$\sigma_L^{3445.3}$	$4.973\sigma_\gamma^{1360} - 0.002\sigma_\gamma^{1771} - 0.005\sigma_\gamma^{3254} - 0.005\sigma_\gamma^{2035} - 0.060\sigma_\gamma^{1852}$	3507–4500

structure evaluation for ^{56}Fe [16]. Our method is based on the observation of at least one γ transition from each level. The level cross section is determined as a difference between the production cross section of the γ's decaying from the level and the γ's feeding the level, with the coefficients calculated based on the branching ratios. Table IV displays all the formulas used.

We were able to detect one γ transition from all excited levels up to the excitation energy of 3500 keV, with the exception of the level at 3076.2 keV. This is the only negative parity state [$J^\pi = (3^-)$] in this excitation energy range. The existence of this level was established using various reactions (pick-up, electron, and α inelastic scattering) with energy resolutions of the order of 30–50 keV. The main argument for the spin assignment is the angular distribution in an (α, α') measurement [49] while the only γ spectroscopy experiments confirming the level and its γ decay are based on proton capture [50,51]. However, the existence of the 3076.2-keV level is questioned by several recent studies using neutron inelastic scattering [52,53] or fusion-evaporation reactions [54]. We did not observe the 3076.2-keV level despite the fact that the TALYS 1.6 calculation indicates a level production cross section that reaches a maximum of ≈ 120 mb for $E_n \approx 5$ MeV, thus comparable to the 2960.0-keV level. Above 3500 keV we were also able to detect at least one γ decay from most of the excited states up to the excitation energy of 4500 keV, but we observed very few transitions occurring at higher excitation energies.

Therefore we calculated the cross section for the first ten excited levels (with the exception of the 3076.2-keV level) and we consider that our results are precise (within the uncertainty limits) up to $E_n = 4.5$ MeV. Above this limit the values we calculate represent only lower limits of the total inelastic cross section and upper limits in case of the level cross section. We choose to present the total inelastic cross section for energies up to 18 MeV, but we restrict the level cross sections to the energy range up to 4.5 MeV.

The total neutron inelastic cross section is displayed in Fig. 11. For comparison purposes, we show also the cross section from the JEFF 3.1.2 and ENDF/B-VII.1 data bases which represent an evaluated average of the previous experimental results.

TABLE V. The level density in the compound nucleus ^{57}Fe calculated using the BSFG model compared with the number of resonances counted from the total inelastic cross section.

E_n range (MeV)	E_n^{avg} (MeV)	$E*(^{57}\text{Fe})$ (MeV)	J^π in ^{57}Fe (TALYS)	Level density (BSFG) (1/MeV)	Level density (Exp.) (1/MeV)
0.9–1.4	1.15	8.78	1/2–5/2	158	134
1.4–1.9	1.65	9.27	1/2–5/2	205	94
1.9–2.4	2.15	9.76	1/2–5/2	265	60
2.4–2.9	2.65	10.25	1/2–5/2	343	52
2.9–3.4	3.15	10.74	1/2–5/2	441	46
3.4–3.9	3.65	11.23	1/2–7/2	858	28

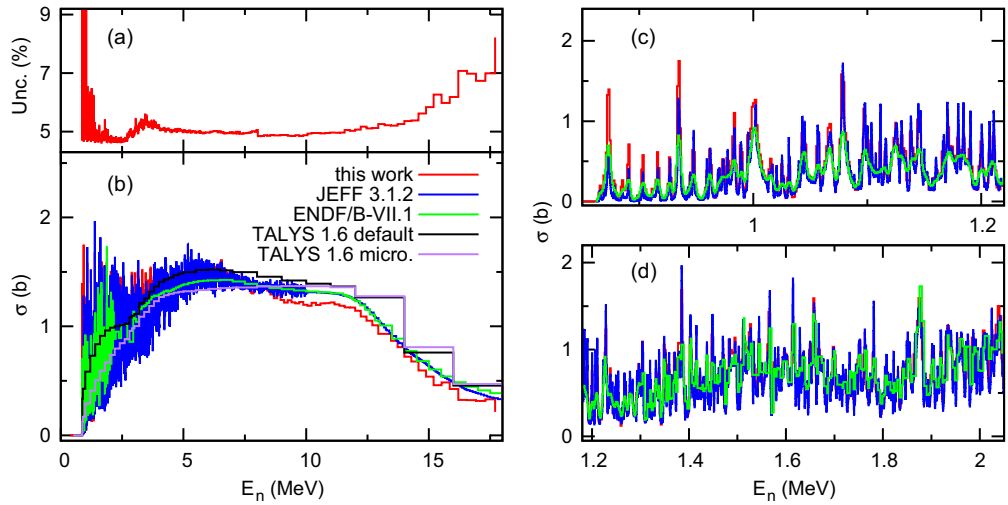

FIG. 11. (Color online) Total neutron inelastic cross section of ^{56}Fe. Panel (b) compares the total neutron inelastic cross section obtained in the present measurement with the evaluated data and with the TALYS 1.6 calculations for the full energy range while panel (a) displays the corresponding uncertainties. Below 2.5 MeV the relative uncertainty peaks when the cross section is low. Panels (c) and (d) show a zoom of the $E_n < 2$ MeV region. Above $E_n \approx 6$ MeV the observed fluctuations are dominated by counting statistics.

The total inelastic cross section starts at the threshold ($E_n^{\text{th}} = 862$ keV) and resonant structures are visible up to $E_n = 6$–7 MeV. As this makes the direct comparison between our data, evaluations, and the TALYS 1.6 calculations difficult, we present also in Figs. 11(c) and 11(d) a zoom over the neutron energy range up to 2 MeV. The cross section grows as the neutron energy increases up to about 1.5 b for $E_n =$ 5–12 MeV and decreases for more energetic neutrons as the $(n, 2n)$ channel opens at 11.4 MeV. Above $E_n = 6$–7 MeV the observed fluctuations become smaller than the experimental uncertainty.

The total inelastic cross section is dominated by the γ transition between the first excited level and the ground state $E_\gamma = 846.8$ keV. Consequently, the differences observed in Fig. 7 between our result and the previous experimental data are also visible here, mostly in the neutron energy range above 8 MeV.

Finally, Fig. 12 compares the level production cross sections deduced from our measurement to TALYS calculations. Like in the case of γ production cross sections, the default TALYS 1.6 calculation reproduces generally better the experimental values than the microscopic calculation. A very good overlap between the experimental data and the default TALYS calculation is seen especially for the cross section of the first two excited levels, $E_L = 846.8$ and 2085.1 keV. The agreement seems to be much poorer for the $E_L = 3123.0$ keV level, but this was expected since the γ transition with $E_\gamma = 1037.8$ keV depopulating this level is also poorly reproduced by TALYS 1.6. We notice again that the microscopic choice of parameters does not bring an improvement of the data description.

E. Level density in ^{57}Fe

Before concluding, we briefly discuss the resonant structures observed in various cross sections at low neutron energies. These are, in principle, related to the level structure in the compound nucleus ^{57}Fe excited beyond the neutron separation energy S_n (more precisely, the excitation energy in the compound nucleus $E^*(^{57}\text{Fe})$ is the sum of S_n and the neutron energy in the center-of-mass system E_n^{CM}, the mass values and S_n being taken from Ref. [55]). Therefore, the number of resonances directly counted in the total inelastic cross section (Fig. 11) was compared to the theoretical level density in ^{57}Fe. The calculations were performed using the backshifted Fermi gas (BSFG) model with only two free parameters, the level density parameter and the excitation energy shift. We used the approach described in Ref. [56] with the parameters determined in Ref. [57]. The angular momenta of the states populated in the compound nucleus in the ^{56}Fe(n, n') reaction were determined using the TALYS 1.6 calculations.

The results are displayed in Table V and they show that, already in the first 0.5-MeV range after the threshold the number of resonances we observe is lower than the theoretically predicted level density. As the energy increases this discrepancy becomes larger. We conclude therefore that for the first few hundred of keV the resonances observed in our cross sections may correspond, at least partially, to individual excited states in the compound nucleus while at higher neutron energies this is not the case anymore and overlap dominates. Above $E_n = 1.4$ MeV these structures should simply be interpreted as Ericson fluctuations [58].

V. CONCLUSION

We measured the γ production, level production, and total inelastic cross sections for the ^{56}Fe isotope using time of flight and γ spectroscopy techniques. Twenty γ production cross sections were determined for incident neutron energies from threshold up to 18 MeV. Also, six γ production cross sections were determined for the $(n, 2n\gamma)$ channel. The level production cross section was built for ten excited levels in ^{56}Fe from threshold up to 4.5 MeV.

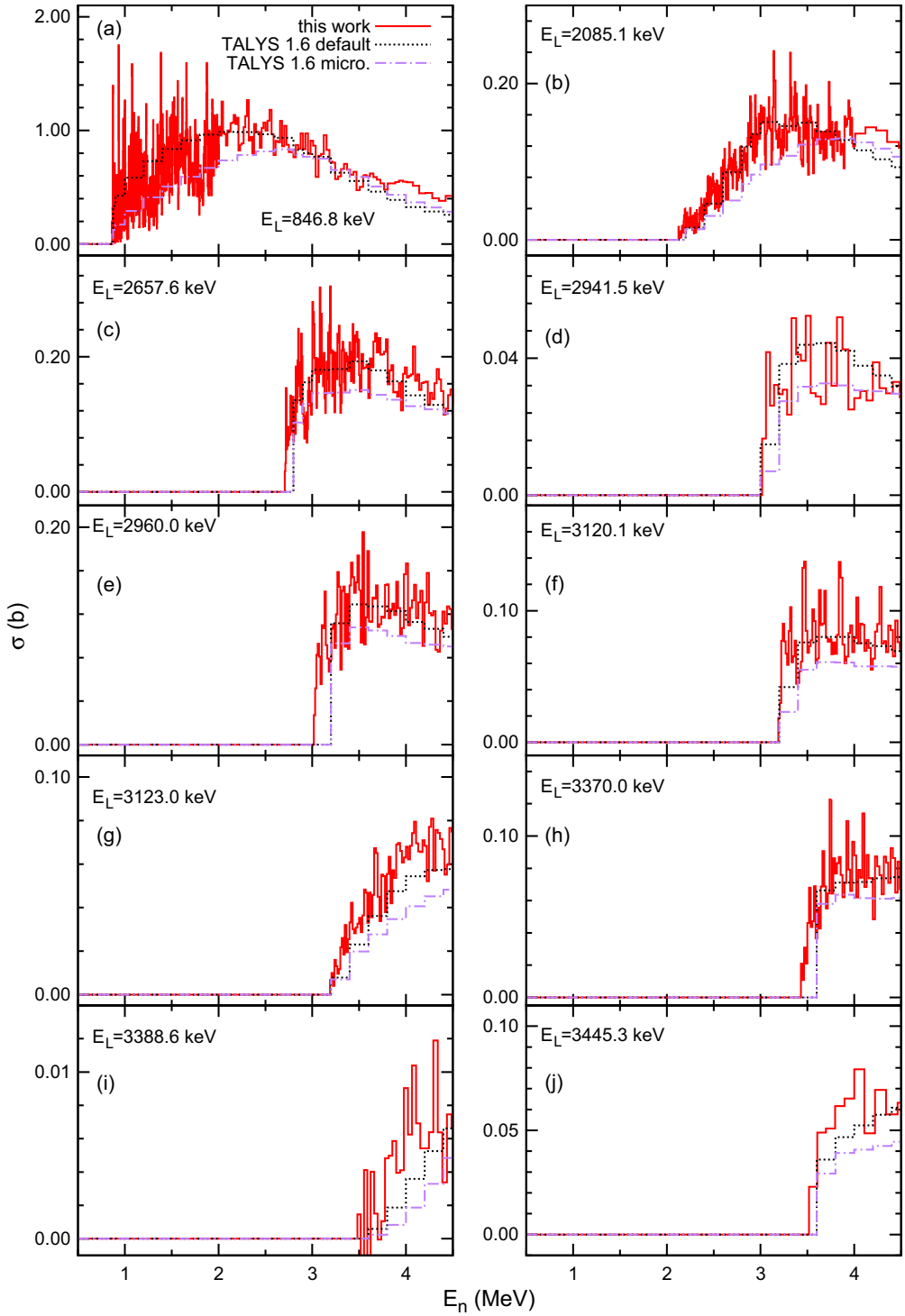

FIG. 12. (Color online) Level cross section for the ^{56}Fe$(n, n\gamma)^{56}$Fe reaction.

We compared our results to previous measurements and with theoretical calculations performed with TALYS 1.6 and concluded that the default parameters of TALYS produce better results than those deduced from microscopic models. In a few cases, discrepancies between the experimental results and the microscopic approach in TALYS were interpreted as a sign of the difficulties encountered by the theory when describing the ^{56}Fe nucleus.

A good overall agreement was found with the previous measurements. However, we observe some differences, like in the case of the strongest γ transition at 846.8 keV that is the main component of the total inelastic cross section.

The accurate cross sections obtained in this work are an important step towards improved accuracy estimates in neutron transport calculations.

ACKNOWLEDGMENTS

The authors thank the team of operators of the GELINA facility for the preparation of the neutron beam and to the technical staff of IRMM, especially to J. C. Drohé, for their support during the commissioning of GAINS and during the data taking campaign. This work was partially supported by the European Commission through the EUROTRANS (Contract No. FP6-FI6W-CT-2004-516520) and ANDES (EURATOM Contract No. FP7-249671) projects.

[1] G. Aliberti, G. Palmiotti, M. Salvatores, and C. G. Stenberg, Nucl. Sci. Eng. **146**, 13 (2004).

[2] G. Aliberti *et al.*, Ann. Nucl. Energy **33**, 700 (2006).

[3] J. K. Böhlke, J. R. de Laeter, P. De Bièvre, H. Hidaka, H. S. Peiser, K. J. R. Rosman, and P. D. P. Taylor, J. Phys. Chem. Ref. Data **34**, 57 (2005).

[4] Request ID 34 of the NEA Nuclear Data High Priority Request List, http://www.nea.fr/html/dbdata/hprl/hprlview.pl?ID=454.

[5] G. Aliberti, G. Palmiotti, and M. Salvatores, in *Proceedings of the CANDIDE workshop on Neutron Measurements Evaluations and Applications, NEMEA-4, October 16–18 2007, Prague, Czech Republic*, edited by A. Plompen (Publications Office of the European Union, Luxembourg, 2008), p 127.

[6] D. E. Lea, Proc. Royal Soc. London A **150**, 637 (1935).

[7] R. B. Day, Phys. Rev. **102**, 767 (1956).

[8] F. G. Perey, W. E. Kinney, and R. L. Macklin, in *Proceedings of the Third Conference on Neutron Cross Sections and Technology, March 15–17, 1971, Knoxville, Tennessee, USA*, edited by R. L. Macklin (National Technical Information Service, US Department of Commerce, Washington, DC, 1971), Vol. 1, p. 191.

[9] D. L. Smith, ANL/NDM-20 Report of Argonne National Laboratory, Argonne, Illinois, USA (1976).

[10] J. K. Dickens, J. H. Todd, and D. C. Larson, Oak Ridge National Laboratory Technical Report ORNL-TM-11671, 30 (1990).

[11] R. O. Nelson, N. Fotiades, M. Devlin, J. A. Beckerand, P. E. Garrett, and W. Younes, in *Proceedings of the International Conference on Nuclear Data for Science and Technology - ND2004, September 26–October 1, 2004, Santa Fe, USA*, edited by R. C. Haight, M. B. Chadwick, T. Kawano, and P. Talou, AIP Conf. Proc. No. 769 (AIP, New York, 2005), p. 838.

[12] R. Beyer *et al.*, Nucl. Phys. A **927**, 41 (2014).

[13] C. Y. Fu, C. M. Perey, D. M. Hetrick, and F. G. Perey, ENDF/B/VI.1 Evaluation of $n + 56$Fe (1991).

[14] V. Pronyaev, S. Tagesen, H. Vonach, and S. Badikov, Physik Daten 13-8 (1995).

[15] E. Dupont, P. Ribon, H. Weigmann, and G. Vanpraet, in *Proceedings of the International Conference on Nuclear Data for Science and Technology, May 19–24, 1997, Trieste, Italy*, edited by G. Reffo, A. Ventura, and C. Grandi, Conference Proceedings Vol. 59 (Italian Physical Society, SIF, Bologna, 1997), p. 529.

[16] H. Junde, H. Su, and Y. Dong, Nucl. Data Sheets **112**, 1513 (2011).

[17] L. C. Mihailescu, L. Olah, C. Borcea, and A. J. M. Plompen, Nucl. Instrum. Meth. Phys. Research A **531**, 375 (2004).

[18] D. Tronc, J. M. Salomé, and K. Böckhoff, Nucl. Instrum. Meth. Phys. Research A **228**, 217 (1985).

[19] D. Ene, C. Borcea, S. Kopecky, W. Mondelaers, A. Negret, and A. J. M. Plompen, Nucl. Instrum. Meth. Phys. Research A **618**, 54 (2010).

[20] A. Negret, C. Borcea, J. C. Drohe, L. C. Mihailescu, A. J. M. Plompen, and R. Wynants, in *Proceedings of the International Conference on Nuclear Data for Science and Technology—ND2007, April 22–27, 2007, Nice, France*, edited by O. Bersillon, F. Gunsing, E. Bauge, R. Jacqmin, and S. Leray (EDP Sciences, Les Ulis, France, 2008), p. 1015.

[21] A. Negret, C. Borcea, Ph. Dessagne, M. Kerveno, N. Nankov, M. Nyman, A. Olacel, A. J. M. Plompen, and C. Rouki, Nucl. Data Sheets **119**, 179 (2014).

[22] L. C. Mihailescu, C. Borcea, and A. J. M. Plompen, Nucl. Instrum. Meth. Phys. Research **A578**, 298 (2007).

[23] A. J. M. Plompen *et al.*, J. Korean Phys. Soc. **59**, 1581 (2011).

[24] M. B. Chadwick *et al.*, Nucl. Data Sheets **112**, 2887 (2011).

[25] L. C. Mihailescu, C. Borcea, A. J. Koning, and A. J. M. Plompen, Nucl. Phys. A **786**, 1 (2007).

[26] L. C. Mihailescu, C. Borcea, A. J. Koning, A. Pavlik, and A. J. M. Plompen, Nucl. Phys. A **799**, 1 (2008).

[27] L. C. Mihailescu *et al.*, Nucl. Phys. A **811**, 1 (2008).

[28] C. Rouki *et al.*, Nucl. Instrum. Meth. Phys. Research A **672**, 82 (2012).

[29] C. Rouki, A. R. Domula, J. C. Drohe, A. J. Koning, A. J. M. Plompen, and K. Zuber, Phys. Rev. C **88**, 054613 (2013).

[30] A. Negret, C. Borcea, and A. J. M. Plompen, Phys. Rev. C **88**, 027601 (2013).

[31] A. Negret *et al.*, Phys. Rev. C **88**, 034604 (2013).

[32] J. F. Briesmeister, Los Alamos National Laboratory Report No. LA-13709-M (2000).

[33] D. Deleanu, C. Borcea, Ph. Dessagne, M. Kerveno, A. Negret, A. J. M. Plompen, and J. C. Thiry, Nucl. Instrum. Methods Phys. Research A **624**, 130 (2010).

[34] A. J. M. Plompen *et al.*, JRC Scientific and Policy Report EUR 26194 EN, ISBN 978-92-79-33383, Publication Office of the European Union, Luxembourg, 2013.

[35] G. Fehrenbacher, R. Meckbach, and H. G. Paretzke, Nucl. Instrum. Methods Phys. Research A **372**, 239 (1996).

[36] A. J. Koning, S. Hilaire, and M. C. Duijvestijn, in *Proceedings of the International Conference on Nuclear Data for Science and Technology - ND2007, April 22–27, 2007, Nice, France*, edited by O. Bersillon, F. Gunsing, E. Bauge, R. Jacqmin, and S. Leray (EDP Sciences, Les Ulis, France, 2008), p. 211.

[37] TALYS 1.6 manual, http://www.talys.eu.

[38] J. Raynal, CEA Saclay Report No. CEA-N-2772 (1994).

[39] A. J. Koning and J. P. Delaroche, Nucl. Phys. A **713**, 231 (2003).

[40] E. Bauge, J. P. Delaroche, and M. Girod, Phys. Rev. C **63**, 024607 (2001).

[41] E. M. Cornelis, L. Mewissen, and F. Poortmans in *Proceedings of the International Conference on Nuclear Data for Science and Technology, September 6–10, 1982, Antwerp, Belgium*, edited by K. H. Bockhoff (Springer, Netherlands, 1984), p. 135.

[42] J. A. Harvey, private communication for the EXFOR entry no. 13764.001.

[43] R. Capote *et al.*, Nucl. Data Sheets **110**, 3107 (2009).

[44] A. J. Koning, S. Hilaire, and S. Goriely, Nucl Phys. A **810**, 13 (2008).

[45] S. Goriely, S. Hilaire, and A. J. Koning, Phys. Rev. C **78**, 064307 (2008).
[46] J. Kopecky and M. Uhl, Phys. Rev. C **41**, 1941 (1990).
[47] S. Goriely, E. Khan, and M. Samyn, Nucl. Phys. A **739**, 331 (2004).
[48] A. J. Koning and D. Rochman, Nucl. Data Sheets **113**, 2841 (2012).
[49] G. Bruge, J. C. Faivre, H. Faraggi, and A. Brussiere, Nucl. Phys. A **146**, 597 (1970).
[50] Z. Guo, C. Alderliesten, C. van der Leun, and P. M. Endt, Nucl. Phys. A **540**, 117 (1992).
[51] M. Krtička, J. Lipták, J. Materna, F. Šterba, J. Šterba, J. Vrzal, and M. Wintrová, Czechoslovak J. Phys. **53**, 483 (2003).
[52] A. M. Demidov, L. I. Govor, V. A. Kurkin, and I. V. Mikhailov, Phys. At. Nucl. **67**, 1884 (2004).
[53] N. Fotiades, R. O. Nelson, and M. Devlin, Phys. Rev. C **81**, 037304 (2010).
[54] D. E. Appelbe *et al.*, Phys. Rev. C **62**, 064314 (2000).
[55] M. Wang, G. Audi, A. H. Wapstra, F. G. Kondev, M. MacCormick, X. Xu, and B. Pfeiffer, Chin. Phys. C **36**, 1603 (2012).
[56] T. von Egidy and D. Bucurescu, J. Phys.: Conf. Series **338**, 012028 (2012).
[57] T. von Egidy and D. Bucurescu, Phys. Rev. C **72**, 044311 (2005).
[58] T. Ericson, Ann. Phys. (NY) **23**, 390 (1963).